Int. J. Heat Mass Transfer. Vol. 30, No. 1, pp. 23–41, 1987
Printed in Great Britain

0017–9310/87 $3.00 + 0.00
Pergamon Journals Ltd.

Turbulent heat and momentum transfer of combined forced and natural convection along a vertical flat plate—aiding flow

K. KITAMURA and T. INAGAKI

Department of Energy Engineering, Toyohashi University of Technology, Tempaku-cho, Toyohashi 440, Japan

(*Received* 25 *July* 1985 *and in final form* 2 *April* 1986)

Abstract—An aiding flow of turbulent, combined convection along a vertical flat plate is investigated experimentally in the range of high values of Rax^* and Rex numbers. Local Nusselt numbers in the combined convection region are found to decrease as much as 25% than those for the pure forced and natural convection. It is revealed from the measurements of velocity and temperature that the reductions in heat transfer are mainly caused by the turbulent suppression. Turbulent transport mechanisms within the combined convective boundary layers are also discussed from the visualized data of the flow and temperature fields over the test plate.

1. INTRODUCTION

COMBINED forced and natural convective flow along a vertical flat plate is encountered in a wide variety of heat transfer equipment and environmental situations. A number of studies have, therefore, been carried out to investigate their heat transfer characteristics. However, most concern has been paid to laminar combined convection, while very little information was obtained with turbulent combined convection. This is mainly because of the fact that the turbulent combined flow can only be realized in the region of high Rayleigh (Rax) and Reynolds (Rex) numbers, and such experimental conditions are difficult to attain in a laboratory framework. Furthermore, the lack of experimental data has hampered the analytical studies of turbulent combined convection.

Hall and Price [1] first conducted the experiments on an ascending air flow of turbulent combined convection over an isothermally heated, vertical plate. They found that the wall temperatures in a turbulent regime initially increase and then decrease as the forced flow velocity is increased. This result may suggest the occurrence of minimum heat transfer in the combined convection region but will not be of much use for further discussion, because the heat transfer coefficients have not been obtained. Oosthuizen [2] has performed the numerical study of an aiding flow of turbulent combined convection. The effect of the buoyancy force on the turbulent terms has been accounted for using a mixing length model. However, it is uncertain whether his analysis can predict the heat transfer behavior of combined convection or not, since the relevant experimental data of heat transfer have not been available.

On the other hand, the heat transfer experiments on the turbulent combined flow in a vertical pipe have been conducted by several workers. Petukhov and Sporygin [3], Watts and Chou [4], and a few others have revealed the marked reduction in heat transfer for an ascending water flow in a heated pipe. These results together with the data for a descending flow in a heated pipe were reviewed by Petukhov *et al.* [5].

The reduced heat transfer for ascending pipe flow has been observed when the Nusselt numbers at specific Grashof numbers are compared with those for pure forced convection under the same Reynolds number. For the sake of the above comparison, the Reynolds number should be kept constant throughout the run with different Grashof numbers. Nevertheless, the flow rate through a vertical pipe and, therefore, the Reynolds number are inevitably increased by an increase in the Grashof numbers, so that the pressure drop between the inlet and outlet of the test pipe was adjusted to maintain the constant flow rate and Reynolds number. However, the change in the pressure drop will alter the flow field substantially, and then the heat transfer of combined convective flow. This change in pressure drop might have caused the reductions in heat transfer and also the complicated behavior of heat transfer for an ascending flow in a heated pipe. Although these studies are important in view of the practical application of turbulent combined convection, their results cannot provide the basic information about the turbulent transport of combined convection itself. On the contrary, boundary-layer flows are free from the above restrictions. The fundamental nature of the turbulent combined convection will, therefore, be revealed by the experiments on the boundary-layer flow.

On the basis of the above discussion, the present experiments have been performed on the turbulent aiding flow of combined forced and natural convection. Turbulent fluid flow and heat transfer are both treated in the high Rayleigh (Rax^*) and Reynolds (Rex) numbers region, where no quantitative data

NOMENCLATURE

f	frequency of streak
g	gravitational acceleration
Grx^*	modified Grashof number, $g\beta q_w X^4/\kappa\nu^2$
h	heat transfer coefficient, $q_w/(T_w - T_\infty)$
K	acceleration parameter, $(\nu/U_\infty^2)(\mathrm{d}U_\infty/\mathrm{d}X)$
Nux	Nusselt number, hX/κ
Pr	Prandtl number, ν/α
q	heat flux
Rax^*	modified Rayleigh number, Grx^*Pr
Rex	Reynolds number, $U_\infty X/\nu$
T	time-averaged temperature
t'	temperature fluctuation
U	time-averaged streamwise velocity
u'	streamwise velocity fluctuation
u^*	friction velocity, $\sqrt{\tau_w/\rho}$
v'	normal velocity fluctuation
X	height from the leading edge of the plate
Y	distance from the wall
Z	spanwise distance.

Greek symbols

α	thermal diffusivity of fluid
β	coefficients of volume expansion
λ	spanwise distance between streaks
λ^+	non-dimensional streak spacing, $\lambda u^*/\nu$
$\hat{\lambda}$	non-dimensional streak spacing, $(g\beta q\lambda^4/\kappa\nu^2)_w^{1/4}$
κ	thermal conductivity of fluid
ν	kinematic viscosity of fluid
ρ	density of fluid
τ	shear stress
δ	boundary-layer thickness
ζ	non-dimensional parameter, $(Grx^*/NuxRex^{2.7})$.

Superscripts

$\bar{}$	time-averaged value
$\tilde{}$	r.m.s. value.

Subscripts

c	at duct center
f	pure forced convection
fm	at film temperature
n	pure natural convection
w	at wall
X	at location X
∞	at main stream.

have been available at present. Since such experimental conditions are difficult to attain, specially designed apparatus was installed and water was adopted as a working fluid.

Local heat transfer coefficients in each regime of forced, natural and their combined convection are measured in the range of maximum $Rax^* \simeq 6 \times 10^{16}$, and $Rex \simeq 10^6$. The quantitative data of the velocity and temperature distributions and their turbulent fluctuations are also obtained to investigate the structure of a turbulent combined convective boundary layer.

A recent paper [6] by one of the present authors has revealed that the ordered motion of the large scale eddies plays an important role on the heat and momentum transport within the turbulent boundary layer of natural convection. Furthermore, it has been recognized that the ordered motion of large scale eddies, so-called bursting phenomena, exists in a turbulent boundary layer of forced convection and governs the turbulent transport. It should be considered from the above facts that these large eddies also appear in the boundary layer of combined convection and will exert a serious influence on the turbulent transport.

In order to investigate the large eddy motion, the temperature distributions on the heated surface and the flow field near the test plate are visualized by using a liquid crystal sheet and a hydrogen-bubble method, respectively.

2. EXPERIMENTAL APPARATUS AND MEASUREMENT

2.1. *Apparatus*

A schematical illustration of the experimental apparatus is presented in Fig. 1. The rectangular duct of $300 \times 300\ \mathrm{mm}^2$ cross-sectional area and of 3.6 m height was adopted as a test duct, into which a forced main stream of water flowed. This duct was set up vertically and submerged into the large reservoir $3 \times 1.5\ \mathrm{m}^2$ in area and 6.3 m in depth. A nozzle of 9:1 contraction ratio was fitted to the inlet of the duct so as to obtain a uniform, vertical flow at the duct inlet and to reduce the turbulence level of the main flow. The bottom edge of the nozzle was placed 1 m from the floor to inhibit the harmful disturbances introduced into the main flow. The flow passed through the duct, entered the suction port of a pump, and returned into the reservoir.

A flow rate was measured by a pre-calibrated Waltmann flow meter and was adjusted by the flow control valves. The return headers were installed around the inner periphery of the reservoir. By the use of the above apparatus and the deep and large volume reservoir, a uniform main flow of maximum turbulent intensity less than 3% was attained at the inlet of the duct, and the temperature rise of the main stream was kept within $0.25\ \mathrm{K\ h^{-1}}$ during the heat transfer experiments.

The test duct was constructed with three acrylic resin plates 10 mm in thickness and with a plywood

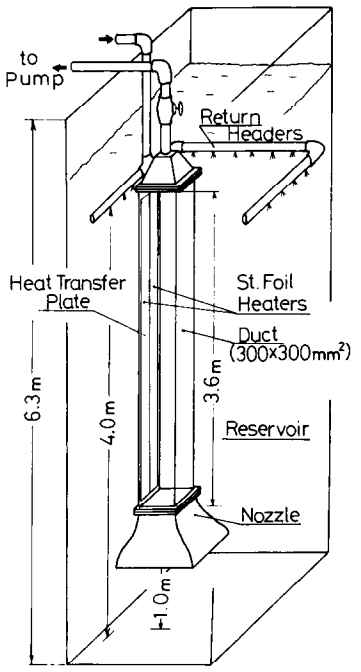

FIG. 1. Experimental apparatus.

plate 15 mm in thickness. The heat transfer plate consisted of the above plywood plate and stainless-steel foil heaters 30 μm thick, 3.5 m long, and 135 mm wide. The heaters were glued on the surface of the plywood plate and were connected in series. They were heated by an AC power supply to obtain a uniform heat flux throughout the test surface. The surface temperatures of the heated plate were measured by chromel–alumel thermocouples of 70 μm diameter, which were spot welded on the back of the heater at constant intervals of 200 mm along the vertical line, which is located 30 mm from the center-line of the test plate. The heat lost by conduction through the plywood plate and by radiation from the heaters was estimated to be less than 3.5% of the total surface heat flux. This value is negligibly small, and therefore, the wall heat flux was calculated from the electrical input to the heater.

The experiments were conducted within the temperature range of the main stream T_∞ from 26 to 28°C and of the heated surface T_w from 30 to 46°C. The maximum temperature differences between the wall and the main stream were kept within 20 K throughout the experiments in order to lessen the influence of property variations on the heat transfer. The thermophysical properties in Rex, Grx^*, Nux and Pr were estimated at the film temperature $T_{fm} = (T_w + T_\infty)/2$.

2.2. *Measurements of velocity and temperature*

The time-averaged velocity and temperature and their fluctuations were measured with a constant temperature, hot-film anemometer and a constant current thermometer. A quartz-coated, double wire, hot-film probe (Thermo-System Inc., No. 1244-60W) was used for the measurements of both velocity and temperature. Output signals both from the anemometer and the thermometer were simultaneously recorded and digitized by a digital data recorder. These digital data were transferred to a personal computer, and were converted into the real velocities and temperatures by using the pre-calibrated relations between the output voltages and the velocities–temperatures. Then, the time-averaged velocities and temperatures and their root-mean-square (r.m.s.) values of fluctuations were numerically computed.

In order to check the influences of sampling frequencies fr and numbers of sampling data nd on the above data, the values fr and nd have been varied systematically in the range of $fr = 10 \sim 100$ Hz and $nd = 1024 \sim 8192$, where $fr = 100$ Hz is the upper limit of the probe response. The results obtained with different values of fr and nd under the same experimental conditions were compared with each other, and it was revealed that the values $fr = 20$ Hz and $nd = 4096$ are large enough to obtain reproducible results. Further increase in fr and nd gave only $\pm 2\%$ deviation against the mean of time-averaged values, and also somewhat larger deviation less than $\pm 5\%$ against the mean values was obtained with r.m.s. values. These values were considered to fall within the range of the randomness of turbulence itself. Therefore, most of the present experiments adopt $fr = 20$ Hz and $nd = 4096$ so as to save CPU time and memory size.

2.3. *Preliminary experiments*

For simplicity of the experimental conditions, the turbulent boundary layers developed along a test plate should be two-dimensional, but the boundary layers developed over both side plates may interfere with the above boundary layer owing to the limited size of the duct cross-section. Therefore, in order to confirm the two-dimensionality of the present boundary layer, the mean velocity and its fluctuation intensity distributions across the boundary layer were measured at the location near the duct outlet in the lowest main velocity case.

As one of the typical examples of these data, the streamwise velocity and its r.m.s. intensity distributions are represented in Fig. 2 in the case of $X = 3.2$ m, $Y = 10$ mm and $U_\infty = 2.6$ cm s^{-1}. The local velocities and intensities are normalized by those at the center of the test plate $Z = 0$, and are plotted with the spanwise distance Z from the centerline of the test plate.

The figure indicates that these distributions are uniform over at least a 120 mm span in the central portion of the test plate for both cases of wall heat flux, $q_w = 4000$ W m^{-2} and $q_w = 0$ W m^{-2}. Taking account of the fact that the thickness of isothermal boundary layers developed over both of the side plates

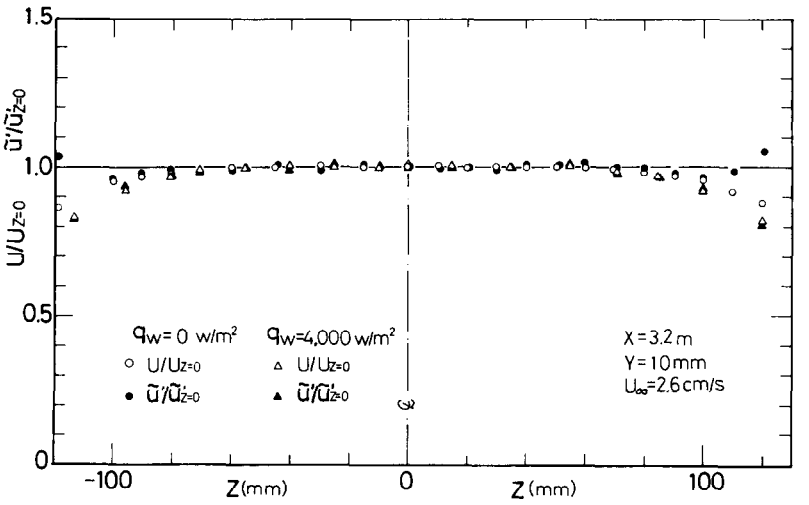

FIG. 2. Streamwise velocity and its fluctuation intensity distributions across the boundary layer.

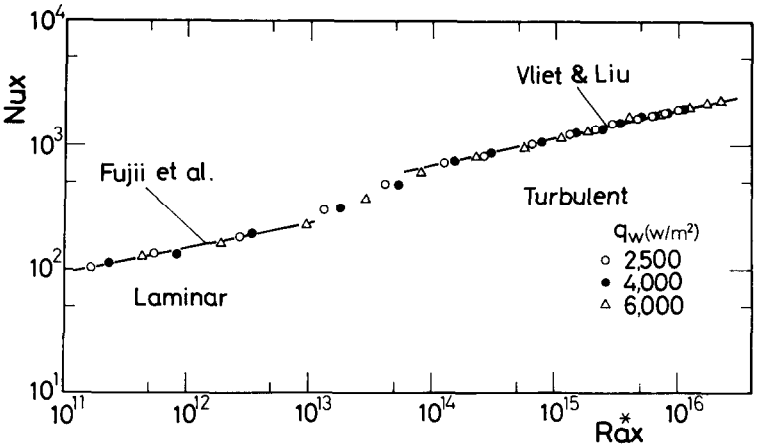

FIG. 3(a). Local Nusselt numbers for a pure natural convection along a vertical flat plate heated with a uniform heat flux.

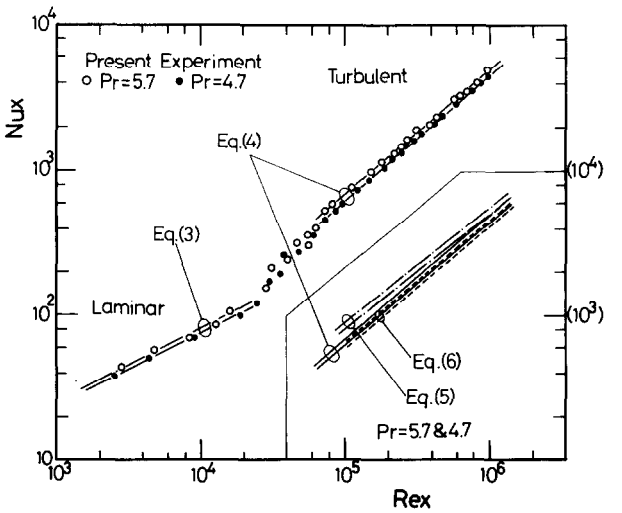

FIG. 3(b). Local Nusselt numbers for a pure forced convection along a vertical flat plate.

is proportional to $X^{4/5}U_\infty^{-1/5}$ and that most of the turbulent data to be mentioned in the next section have been obtained at the locations of smaller X and under higher velocities of main flow U_∞ than those for the above case, the value 120 mm is regarded as an adequate, though not sufficient, length to attain two-dimensional boundary layers.

Another point can also be discussed. The main stream velocity U_∞ increases or, in some cases, decreases in the streamwise direction due to the development of the boundary layers along the test plate and also along the other duct walls. Such acceleration or deceleration of the main flow might exert undesirable influences on the present boundary layer. Therefore, in order to assess the velocity variations, the main stream velocities at $X = 3$ m were monitored with the hot-film probe in all runs of the present experiments, and were compared with those at the duct inlet $X = 0$ m. The results show that the relative increase or decrease in the velocities between two locations $X = 0$ and 3 m does not exceed $\pm 6\%$ even in the most severe cases. Considering this fact, the velocity at the duct inlet is adopted as the representative velocity of the main stream U_∞ in the present study.

The acceleration parameters K were, then, estimated by assuming the linear velocity variations in the X direction, and their absolute values were obtained as less than $K \simeq 4.7 \times 10^{-7}$. These K values are much smaller than $K \simeq 3.6 \times 10^{-6}$, the value found by Kline *et al.* [7] which has been recognized as an onset condition for a laminar retransition. Therefore, it is confirmed that the acceleration or deceleration of the main flow exerts no appreciable influence on the present boundary layer.

3. RESULTS AND DISCUSSION

3.1. *Heat transfer*

Local heat transfer coefficients were first measured along a vertical direction for both cases of pure natural and forced convection. For the experiments of pure natural convection, the nozzle connected with the outlet of the test duct was removed to open the duct to the environment, and the whole duct was submerged into water. The results of the local Nusselt numbers for the pure natural convection are plotted in terms of Rax^* and are shown in Fig. 3(a), where the surface heat fluxes q_w of the test plate are varied. The distance X from the leading edge of the plate is adopted as a characteristic length in Nux and Rax^*. The solid lines in the figure represent the analytical laminar solution by Fujii *et al.* [8], and also the empirical correlation for the turbulent heat transfer by Vliet and Liu [9]. Their correlation equations are expressed as follows:

Fujii *et al.* [8]

$$\text{laminar} \quad Nux = 0.586 Rax^{*0.2}. \tag{1}$$

Vliet and Liu [9]

$$\text{turbulent} \quad Nux = 0.568 Rax^{*0.22}. \tag{2}$$

As shown in the figure, the present data coincide well with the above equations, and the flow regimes are classified as: laminar $Rax^* < 10^{13}$; and turbulent $Rax^* > 10^{14}$.

The data for the forced convection are given in the Rex–Nux plane and are illustrated in Fig. 3(b). The distance X is also employed as a characteristic length in the local Reynolds numbers and Nusselt numbers, since X is the simplest and most universal length scale both for the forced and natural convection.

The values of Nux for pure forced convection depend on Pr as well as Rex. Therefore, the present measurements were performed at $Pr = 5.7$ and $Pr = 4.7$, in order to ascertain the effect of Pr on heat transfer. In particular, the latter Prandtl number, $Pr = 4.7$, was attained by raising the temperature of the main stream up to 34°C. Both data were obtained under the various velocities of the main flow. The maximum temperature difference between the wall and the main stream was kept less than 3 K throughout the run by adjusting the surface heat flux so that the buoyancy force will not affect these heat transfer data.

The heat transfer for a laminar flow over a uniform heat flux wall has been analyzed by Chapman and Rubesin [10], and their correlation equation is expressed by the following equation, which is also shown with the solid lines in the figure

$$Nux = 0.458 Rex^{1/2} Pr^{1/3}. \tag{3}$$

As is obvious from the figure, the present Nusselt numbers are in good agreement with those estimated from equation (3).

The figure also shows that the turbulent flow is realized in the region, $Rex > 6 \times 10^4$, where the values of Nux for $Pr = 5.7$ provide 8–9% larger values than those for $Pr = 4.7$. The above critical Rex for a turbulent transition, $Rex = 6 \times 10^4$, is somewhat smaller than those observed in the previous studies. This is mainly because of high turbulent intensities in the present main flow. Several correlation equations have been proposed for the turbulent heat transfer. In order to check the present turbulent data with the previous results, the following equations are referred and compared

$$Nux = 0.0296 Rex^{0.8} Pr / [1 + 1.54 Pr^{-1/4} \times Rex^{-0.1}(Pr - 1)] \tag{4}$$

$$Nux = 0.0309 Rex^{0.8} Pr^{0.6} \tag{5}$$

$$Nux = RexPr(C_f x/2)^{1/2} / [2.12 \ln(RexC_f x) + 12.5 Pr^{2/3} + 2.12 \ln Pr - 7.2] \tag{6}$$

where

$$(2/C_f x)^{1/2} = 2.5 \ln(RexC_f x) + 2.4. \tag{7}$$

Equation (4) is based on the analysis by Deissler [11], which is also cited in ref. [12]. Equations (5) and (6) were obtained by Reynolds *et al.* [13] and by Kader and Yaglom [14], respectively. These equations are

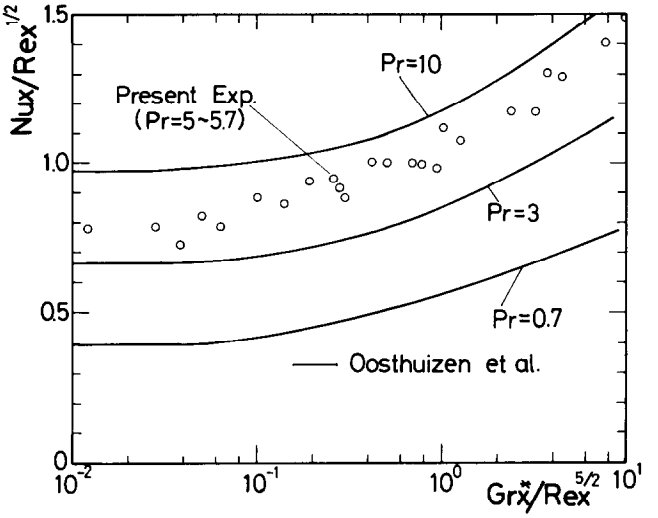

FIG. 4. Non-dimensional heat transfer correlation for laminar combined convection along a vertical flat plate heated with a uniform heat flux.

also illustrated in Fig. 3(b). The Nusselt numbers calculated from equation (5) provide 23–29% larger values than those from equation (4) at $Rex = 10^5$, while the maximum deviation in Nux between equations (4) and (6) is less than 8% within the range of the Rex and Pr shown in the figure. Among these equations, the present turbulent data are fairly well correlated by equation (4) for both values of Pr. Therefore, this equation is adopted as a reference equation which describes the present heat transfer of pure forced convection.

The heat transfer of combined convective flow is investigated in the next place. Before performing the heat transfer experiments, the turbulent and the laminar regions were determined from the output signals of the thermocouples welded behind the heater. The locations where the signals begin to fluctuate were defined here as the onsets of turbulent transition. The local Rax^* and Rex corresponding to the onset are, then, computed from the results obtained under the various values of the main stream velocity and of the surface heat flux. It was revealed that the turbulent transition occurs at the locations where the local Rax^* or Rex exceed either the critical Rax^* or Rex for the pure natural and forced convection. The results also confirm that the laminar flow is preserved only in the region of small X as less than 0.6 m, in most cases of the present experiments.

As was mentioned in Section 1, the analytical studies of laminar combined convective flow along a vertical flat plate have been performed by several workers. In particular, Oosthuizen and Hart [15] have obtained the results with the combined flow along a uniform heat flux wall. The present laminar data are plotted in the $(Grx^*/Rex^{5/2})$–$(Nux/Rex^{1/2})$ plane and are compared with the above analytical solutions as shown in Fig. 4. Solid lines in the figure represent the analytical results for the fluids of $Pr = 0.7$, 3 and 10, and the present laminar data for water of $Pr = 5 \sim 5.7$ are shown with the open circles. The dependency of $(Nux/Rex^{1/2})$ on the parameter $(Grx^*/Rex^{5/2})$ is similar between the analysis and the present experiments. Besides, the values of Nux for the laminar combined flow become much larger than those for the pure forced convection. This enhancement of heat transfer is attributed to the fact that the flow near the wall is accelerated by an imposed buoyancy force.

The heat transfer of turbulent combined flow, on which our main concern is focused, is examined in the next section. From the previous discussion on the

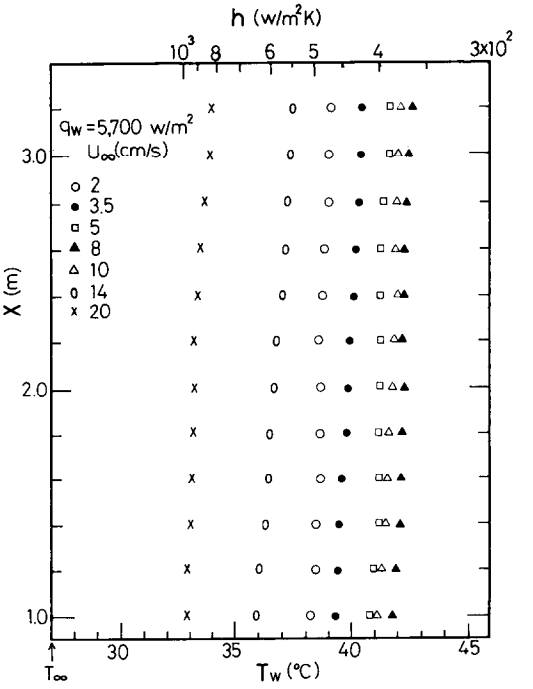

FIG. 5(a). Streamwise distributions of wall temperatures and local heat transfer coefficients under the constant surface heat flux.

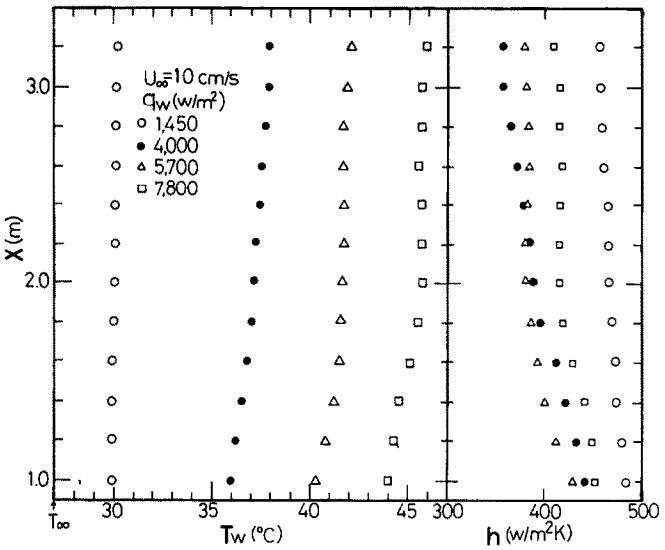

FIG. 5(b). Streamwise distributions of wall temperatures and local heat transfer coefficients under the constant velocity of main stream.

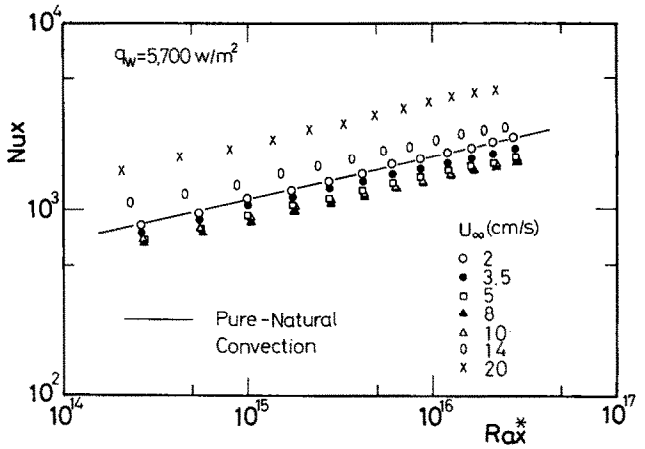

FIG. 6(a). Local Nusselt numbers for a turbulent combined convection under the constant surface heat flux.

turbulent transition, the developed turbulent flow of $Rex > 10^5$ or $Rax^* > 10^{14}$ is mainly treated, and the values are realized in the region of $X > 1$ m in most cases of the present run.

As one of the representative sets of heat transfer data, the wall temperatures and the local heat transfer coefficients were measured in the streamwise direction with the various velocities of the main stream and under fixed surface heat flux. The results obtained with the case of $q_w = 5700\ \mathrm{W\,m^{-2}}$ are presented in Fig. 5(a). The experiments were also conducted under the fixed velocity of the main stream and with several surface heat fluxes. The streamwise distributions of the wall temperatures and the local heat transfer coefficients are given in Fig. 5(b) for the case of $U_\infty = 10\,\mathrm{cm\,s^{-1}}$. The temperature of the main stream is kept constant at $T_\infty = 27°\mathrm{C}$ throughout both series of the run.

Figure 5(a) indicates that the wall temperatures at each location $X > 1$ m increase with the increase in the main stream velocity, and reach the maximum at around $U_\infty = 8\,\mathrm{cm\,s^{-1}}$. Although heat transfer is enhanced in general, by increasing the forced flow velocity, the present results with $U_\infty = 2 \sim 10\,\mathrm{cm\,s^{-1}}$ show a quite opposite and interesting behavior of the heat transfer. Such reductions in heat transfer cannot be explained by the thermal property variations, since the film temperatures change only by 2 K in the above range of U_∞.

These heat transfer data at $X > 1$ m are replotted in the Nux–Rax^* plane as given in Fig. 6(a). The solid line in the figure represents the empirical correlation for pure natural convection expressed by equation (2), and the data at each location $X > 1$ m in Fig. 5(a) shift from left to right in this figure with an increase in the height from the leading edge. The plots for the lowest main velocity, $U_\infty = 2\,\mathrm{cm\,s^{-1}}$, coincide well with equation (2), and the Nux at fixed Rax^* numbers show

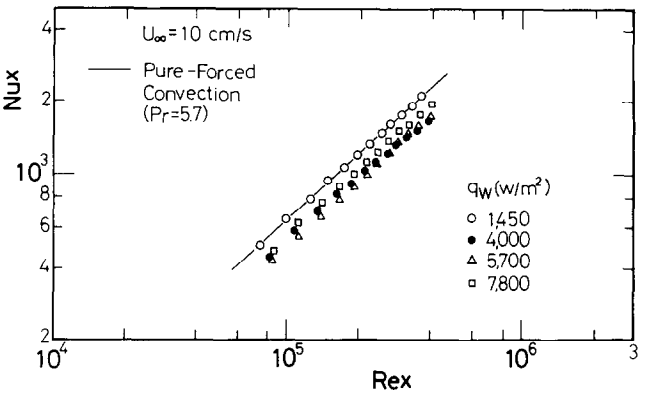

FIG. 6(b). Local Nusselt numbers for a turbulent combined convection under the constant velocity of main stream.

the same heat transfer variations with increasing the main stream velocity as was mentioned in the above. It is confirmed from these data that the heat transfer of turbulent natural convection is inhibited by the imposed forced flow in a certain range of the main flow velocity.

Figure 5(b) demonstrates that the wall temperatures at fixed locations $X > 1$ m increase monotonously with the increase in the surface heat flux, while the local heat transfer coefficients decrease and reach the minimum at $q_w = 4000 \sim 5700\ \mathrm{W\,m^{-2}}$ and then show somewhat larger values at the highest surface heat flux, $q_w = 7800\ \mathrm{W\,m^{-2}}$.

Such reduced heat transfer also appears in Fig. 6(b), where the local Nux calculated from the data at $X > 1$ m in Fig. 5(b) are plotted in terms of the local Rex. The solid line in the figure represents the Rex–Nux correlation for a pure forced convection of $Pr = 5.7$, which is estimated from equation (4). The present data for the smallest heat flux, $q_w = 1450\ \mathrm{W\,m^{-2}}$ and $Pr = 5.7$, are in good agreement with equation (4). The minimum Nux are provided in the range of $q_w = 4000 \sim 5700\ \mathrm{W\,m^{-2}}$. This result shows that the heat transfer of turbulent forced convection is retarded by the induced buoyant flow.

However, the effects of the thermal property variations on these data should be discussed in order to clarify the reduced heat transfer. As seen in Fig. 5(b), the wall temperatures T_w are varied from 30 to 46°C, and the temperature of the main stream T_∞ is kept constant throughout the run at 27°C, and therefore, the film temperatures T_{fm} $[= (T_w + T_\infty)/2]$ change from 28.5 to 36.5°C. With the above increase in the film temperatures, the thermal conductivity κ varies by only 2%, and the kinematic viscosity ν decreases from 0.815×10^{-6} to $0.710 \times 10^{-6}\ \mathrm{m^2\,s^{-1}}$. Thus, the Rex at fixed location X increase by 14.8%, while the Pr decrease from 5.7 to 4.7.

Provided that equation (4) is still valid even in the case of $U_\infty = 10\ \mathrm{cm\,s^{-1}}$ and $q_w = 7800\ \mathrm{W\,m^{-2}}$, the above increase in Rex should lead to Nux larger by 11% for fixed locations X, while the decrease in Pr should offer Nux smaller by 9%; these results were also confirmed in Fig. 3(b). Both values are almost the same and the effects of Rex and Pr on these values of Nux are compensated by each other. Therefore, the present reductions in heat transfer cannot be explained by the property variations and should be attributed to the substantial change in the turbulent transport within the boundary layer of combined convection.

It is worth noting from both Figs. 6(a) and (b) that the local Nux obtained under the certain conditions of U_∞ and q_w, e.g. $U_\infty = 10\ \mathrm{cm\,s^{-1}}$ and $q_w = 5700\ \mathrm{W\,m^{-2}}$, become smaller than those estimated from the empirical correlations for both the pure natural and forced convection. This may result in a marked increase in the surface temperatures, and give rise to serious problems in the design of heat transfer equipment such as high heat flux heat exchangers. Several rearrangements of these heat transfer data were, therefore, performed in order to obtain the non-dimensional correlations for the turbulent combined convective flow, and also to distinguish the flow regimes into the forced, the natural, and their combined convection.

One of the non-dimensional parameters which characterize the combined convective flow is Grx/Rex^2, which represents the ratio of a buoyancy force to an inertia force. The above Grashof numbers is based on the temperature difference between the wall and the environment, and can be transformed into Grx^* by using the relation $Grx = Grx^*/Nux$. The parameter Grx/Rex^2 is expressed as $Grx^*/Nux\,Rex^2$. The local Nusselt numbers obtained from these experiments Nux, were normalized by the Nusselt numbers for the pure forced convection Nux_f, which were calculated from equation (4) under the same values of Rex and Pr as those for the experiments. The ratios Nux/Nux_f exhibit the relative increase or decrease in the heat transfer rate, and are plotted in terms of the above parameter $Grx^*/Nux\,Rex^2$. The results show that most of the minimum values of Nux/Nux_f fall into the range $Grx^*/Nux\,Rex^2 = 1 \sim 10$, which implies that the heat transfer is reduced most significantly in the region where the

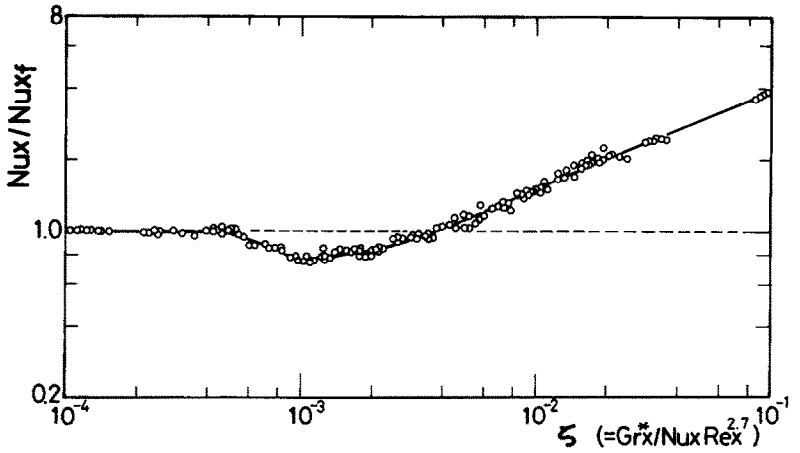

FIG. 7. Non-dimensional heat transfer correlation for a turbulent combined convection along a vertical flat plate. Rearrangement by the parameter (Nux/Nux_f) vs ζ.

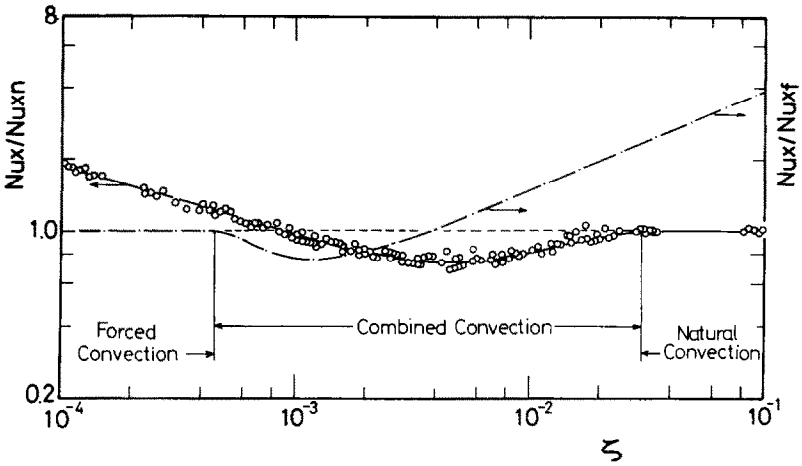

FIG. 8. Non-dimensional heat transfer correlation for a turbulent combined convection along a vertical flat plate. Rearrangement by the parameter (Nux/Nux_n) vs ζ.

buoyancy force and the inertia force are of comparable order of magnitude.

However, these data are scattered and can hardly be correlated with the parameter $Grx^*/NuxRex^2$. Further rearrangements were, therefore, performed by varying the power n in the parameter $Grx/NuxRex^n$ instead of simply setting $n = 2$. The most successful result was obtained with $n = 2.7$ and the present data were replotted in the (Nux/Nux_f)–$(Grx^*/NuxRex^{2.7})$ plane as shown in Fig. 7. The ratios Nux/Nux_f are correlated well with the parameter ζ $(= Grx^*/NuxRex^{2.7})$, and 95% of the total data are collected within the band of $\pm 5\%$ deviation against the mean values. As is demonstrated in the figure, the values of Nux in the range of $\zeta < 4 \times 10^{-4}$ coincide with Nux_f for pure forced convection, and thus, this region is referred to as the forced convection region. In the region of $\zeta > 4 \times 10^{-3}$, the ratios Nux/Nux_f become larger than unity. This result is attributable to the fact that the natural convection is dominant here and much more heat is transferred by natural convection than by pure forced convection. Meanwhile, in the intermediate region between the above two, $4 \times 10^{-4} < \zeta < 4 \times 10^{-3}$, the values of Nux become as much as 25% smaller compared with Nux_f. These results in turn reveal that the parameter ζ can predict satisfactorily the heat transfer behavior of turbulent combined flow.

The rearrangements of the above heat transfer data were also conducted by using the ordinate (Nux/Nux_n) instead of (Nux/Nux_f), where Nux_n are the local Nusselt numbers for the pure natural convection and are estimated from equation (2) under the same values of Rax^* as those for the experiments. The results are presented in Fig. 8 with ζ as an abscissa. Three distinct regions are observed in the figure. The first is the lower ζ region, $\zeta < 9 \times 10^{-4}$, where Nux/Nux_n are larger than unity, and the forced convection is dominant; the second is the intermediate ζ region, $9 \times 10^{-4} < \zeta < 3 \times 10^{-2}$, where Nux/Nux_n are less than unity. The minimum Nux values attained here are as small as 3/4 those of Nux_n for the pure natural convection; and the

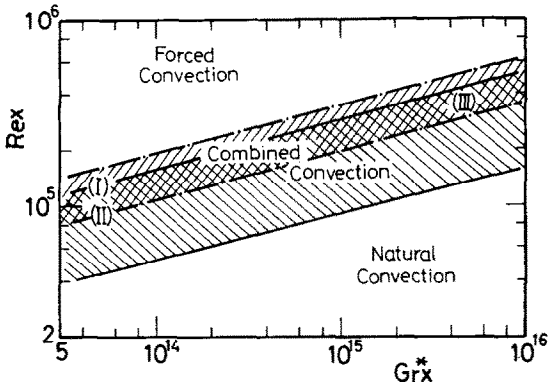

FIG. 9. Classification of the combined convective flow in the Rex–Grx^* plane.

third is the higher ζ region, $\zeta > 3 \times 10^{-2}$, where Nux are equal to Nux_n. This region is, therefore, referred to as the natural convection region.

From the above results in Figs. 7 and 8, the combined convection region is here defined as the region where the local Nux become smaller than either the Nux_f or the Nux_n, so that this region corresponds to the value of ζ as $4 \times 10^{-4} < \zeta < 3 \times 10^{-2}$. In order to clarify three regimes of forced, natural and combined convection, they are mapped in the Grx^*–Rex plane as shown in Fig. 9. Region (I), $4 \times 10^{-4} < \zeta < 4 \times 10^{-3}$, which lies between the dotted lines in the figure, corresponds to the region where the Nusselt numbers are smaller than Nux_f, while in Region (II), $9 \times 10^{-4} < \zeta < 3 \times 10^{-2}$, which is sandwiched in between solid lines, the Nux values become smaller than Nux_n. Furthermore, Region (III), $9 \times 10^{-4} < \zeta < 4 \times 10^{-3}$ gives smaller Nux than both Nux_f and Nux_n.

The forced flow velocity near the vertical wall should be accelerated by the imposed buoyancy force in the case of an aiding flow. This leads to the increase in laminar heat transfer as was mentioned before. However, the turbulent heat transfer rates in the combined convection region are reduced and become considerably smaller than those for pure natural convection as well as pure forced convection. Such reduction in heat transfer should be attributed to a substantial change in the turbulent transport. Therefore, in the next section, the quantitative data of velocity and temperature and of their fluctuations are measured to investigate the turbulent transport within the boundary layer.

3.2. *Velocity and temperature and their fluctuation intensity distributions within the boundary layers*

The present measurements were conducted under the experimental conditions given in Table 1. They consist of following two series of runs. Series A: constant surface heat flux and variable velocities of a main flow; Series B: constant velocity of a main flow and variable surface heat fluxes. All the data were obtained at the location of $X = 3$ m from the leading

Table 1. Experimental conditions for the velocity and temperature measurements

Series	Run	Main velocity, U_∞ (cm s^{-1})	Heat flux, q_w (W m^{-2})	Reynolds number, Rex	Grashof number, Grx^*	Nusselt number, Nux	$Grx^*/NuxRex^{2.7}$, ζ	Boundary-layer thickness, δ (mm)	Thermal boundary-layer thickness, θ (mm)
A	Q1	2.6	4000	7.30×10^4	9.98×10^{14}	1570	4.70×10^{-2}	75	30
A, B	Q2	4.4	4000	12.0×10^4	9.89×10^{14}	1470	1.30×10^{-2}	65	25
A	Q3	9.6	4000	24.8×10^4	9.75×10^{14}	1255	2.12×10^{-3}	30	23
A	Q4	11.2	4000	32.2×10^4	10.1×10^{14}	1550	8.80×10^{-4}	35	25
B	U2	4.4	1000	12.0×10^4	2.26×10^{14}	910	4.80×10^{-3}	35	25
B	U3	4.4	0	12.3×10^4	0	—	0	40	—

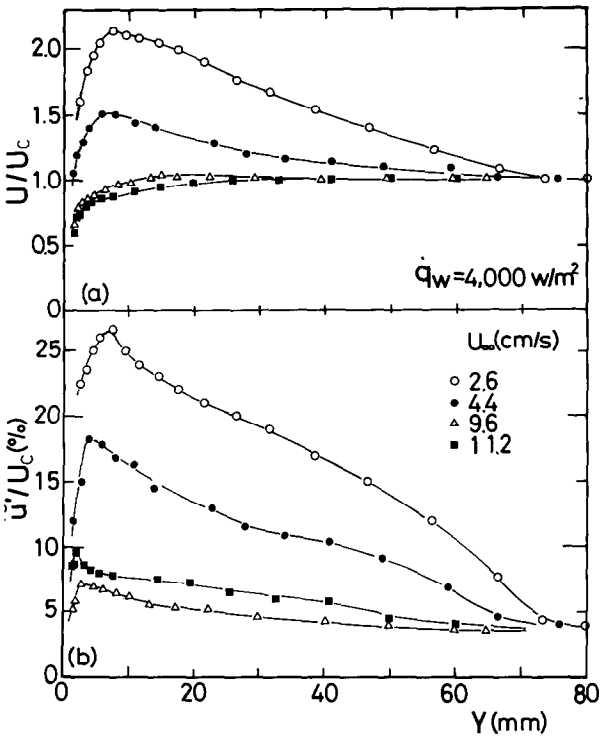

FIG. 10. (a) Time-averaged streamwise velocity distribution and (b) fluctuation intensity distribution of streamwise velocity under the constant surface heat flux. See Table 1 for experimental conditions.

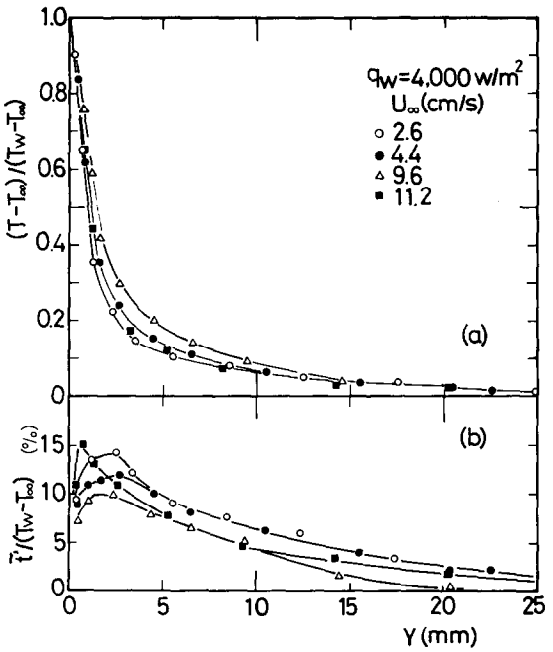

FIG. 11. (a) Time-averaged temperature distribution and (b) intensity distribution of temperature fluctuations under the constant surface heat flux. See Table 1 for experimental conditions.

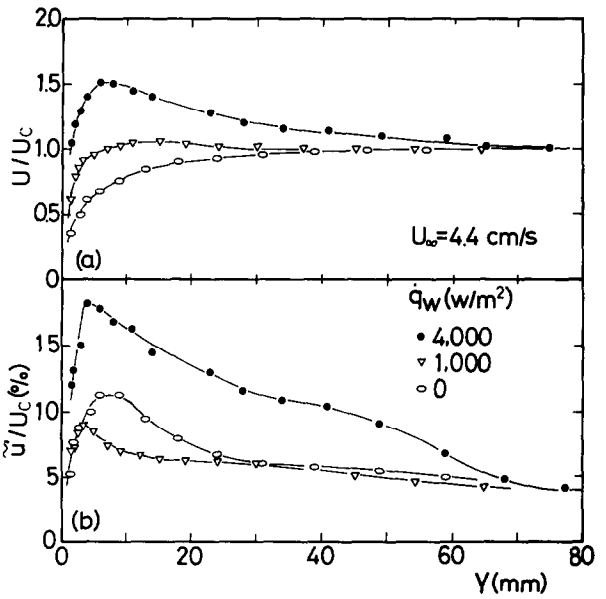

FIG. 12. (a) Time-averaged velocity distribution and (b) fluctuation intensity distribution under the constant velocity of main stream. See Table 1 for experimental conditions.

edge of the heated plate. The above two series A and B are also termed the constant Rax^* and constant Rex experiments, respectively.

Time-averaged streamwise velocity and its fluctuation intensity distributions were obtained in both Series A and B, and are presented in Figs. 10(a), (b) and 12(a), (b), respectively. Figures 11(a) and (b) show the time-averaged temperature and its fluctuation intensity distributions in Series A, respectively. In these figures, the local velocities U and their r.m.s. intensities $\tilde{u}'$ are normalized by the velocity at the duct center U_c, which is almost the same as the main stream velocity U_∞ as was mentioned in Section 2.3. The local temperature differences $(T-T_\infty)$ and their r.m.s. intensities $\tilde{t}'$ are normalized by the temperature difference between the wall and the main stream (T_w-T_∞). The real distance perpendicular to the wall Y is adopted here as an abscissa.

The time-averaged velocity distributions given in Fig. 10(a) show that the maximum velocity reaches twice as much as the velocity at the duct center in the case of $U_\infty = 2.6\,\mathrm{cm\,s^{-1}}$. This peak in the velocity distribution is lowered with an increase in the main stream velocity and can scarcely be observed at $U_\infty = 9.6\,\mathrm{cm\,s^{-1}}$, and then, disappears at $U_\infty = 11.2\,\mathrm{cm\,s^{-1}}$. Furthermore, the boundary-layer thickness δ becomes the largest at the lowest velocity of main flow, and decreases with increasing the main flow velocity. The minimum thickness is attained at $U_\infty = 9.6\,\mathrm{cm\,s^{-1}}$, and further increase in the main stream velocity gives a somewhat larger value of δ. This reduction of δ can be explained by the fact that the velocity at the peak, which is generated by the natural convection, becomes equal to the main velocity of the forced convection as is shown in the figure.

Such variations in the time-averaged velocity distributions are also found in Fig. 12(a). The peak in the velocity distribution is lowered with decreasing surface heat flux, and the velocities at the peak and at the duct center exhibit almost the same value in the case of $q_w = 1000\,\mathrm{W\,m^{-2}}$. The minimum boundary-layer thickness is also attained here. The above experimental conditions of $U_\infty = 9.6\,\mathrm{cm\,s^{-1}}$ and $q_w = 4000\,\mathrm{W\,m^{-2}}$ in Fig. 10(a), and of $U_\infty = 4.4\,\mathrm{cm\,s^{-1}}$ and $q_w = 1000\,\mathrm{W\,m^{-2}}$ in Fig. 12(a) can be plotted within and near the band of Region (III), respectively, where the local Nusselt numbers are smaller than both Nux_f and Nux_n as was mentioned in the previous section. This result in turn indicates that the marked reduction in heat transfer occurs when the velocity at the peak becomes almost equal to the velocity of the main flow.

The streamwise velocity fluctuations shown in Fig. 10(b) take their highest intensities at $U_\infty = 2.6\,\mathrm{cm\,s^{-1}}$, and are reduced significantly with an increase in the main flow velocity. The minimum values are obtained at $U_\infty = 9.6\,\mathrm{cm\,s^{-1}}$ in the entire region of the boundary layer, and then further increase in the main velocity provides somewhat higher intensities. Such variations in the velocity fluctuation are also observed with the experiments of Series B as is illustrated in Fig. 12(b).

By comparing these results with the experimental conditions tabulated in Table 1 and also with the data presented in Fig. 9, it is revealed that the turbulent fluctuations are strongly suppressed in the combined convection region. In particular, the most marked reduction in the intensities appears in Region (III). This accounts for the reduced rate of heat transfer in the combined convection region.

Further evidence to this is given in the time-

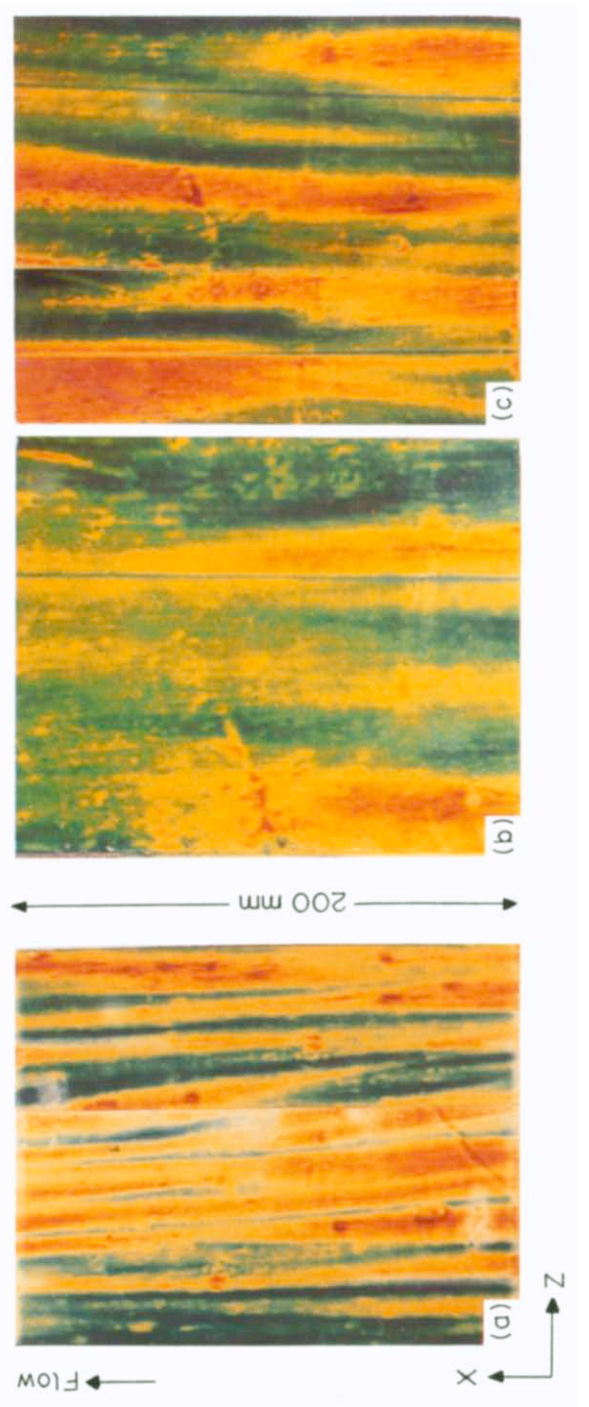

FIG. 13. Visualization of the surface temperature distribution by a liquid crystal sheet. (a) Forced convection: $U_\infty = 14.0\,\mathrm{cm\,s^{-1}}$, $q_w = 7000\,\mathrm{W\,m^{-2}}$, $Rex = 5.42 \times 10^5$, $Grx^* = 3.05 \times 10^{15}$, $\zeta = 3.76 \times 10^{-4}$. (b) Combined convection: $U_\infty = 10.2\,\mathrm{cm\,s^{-1}}$, $q_w = 6000\,\mathrm{W\,m^{-2}}$, $Rex = 3.86 \times 10^5$, $Grx^* = 2.32 \times 10^{15}$, $\zeta = 1.14 \times 10^{-3}$. (c) Natural convection: $U_\infty = 2.5\,\mathrm{cm\,s^{-1}}$, $q_w = 6500\,\mathrm{W\,m^{-2}}$, $Rex = 9.30 \times 10^4$, $Grx^* = 2.62 \times 10^{15}$, $\zeta = 4.82 \times 10^{-2}$.

averaged temperature distributions and also in the intensity distributions of temperature fluctuations, which are shown in Figs. 11(a) and (b), respectively. Figure 11(a) indicates that the temperature gradients in the near-wall region of the boundary layer are most moderate at $U_\infty = 9.6\,\mathrm{cm\,s^{-1}}$. In addition to this, the smallest intensities of the temperature fluctuations also appear at $U_\infty = 9.6\,\mathrm{cm\,s^{-1}}$ in the whole region of the boundary layer. These results are considered as a proof of the turbulence suppression and also of the reduction in heat transfer.

However, the mechanisms of such turbulence suppression have not yet been clarified. Therefore, in the next section, the structure of the turbulent combined convective boundary layer is investigated. Special attention is paid to the different natures between the boundary layers of the forced convection and the natural convection. Furthermore, the turbulent transport within the boundary layer is discussed from the visualized data of the temperature distributions on the heated surface and of the flow field near the test plate.

3.3. *Turbulent transport mechanisms within the boundary layer*

The surface temperature distributions of the heat transfer plate were first visualized by using the liquid crystal sheets, which were patched on the surface of the heater. This visualization technique can be referred to Kasagi [16] or to the previous paper of the authors [6]. The liquid crystal sheet adopted here reflects definite colors at specific ranges of the temperatures. Therefore, the chromel–alumel thermocouples were attached behind the sheet in order to monitor the temperatures of the sheet, and the surface heat flux of the test plate was then adjusted to maintain the constant time-averaged temperature throughout the run.

The typical examples of the visualized photos are presented in Figs. 13(a)–(c) for each region of the forced, combined and natural convection, respectively. These photos were taken at the location of $X = 2.6\,\mathrm{m}$. The yellow or green regions in these photos represent the low temperature regions, where the heat transfer coefficients are large because the plate is heated with a constant heat flux and the temperature of the main stream is kept constant. The blue regions correspond to the high temperature regions, where the heat transfer coefficients are small.

Iritani *et al.* [17] have conducted the similar visualizations in the turbulent boundary layer of forced convection, and found that the streaky patterns, which are featured with the low and the high temperature regions, appear. They also confirmed that the streaky patterns are generated by the bursting phenomena. The present patterns of the surface temperatures in Fig. 13(a) show a notable resemblance to their patterns. The average spacing between the adjacent pairs of these streaks λ was measured with a number of photos taken under the same experimental condition, and was normalized by the friction velocity u^* and the kinematic viscosity ν. Thus, normalized λ^+ $(= \lambda u^*/\nu)$ becomes 92 in the present case, which is almost the same as the mean streak spacing $\lambda^+ \simeq 100$ for the bursting phenomena.

The surface temperature distributions in the natural convection region also represent the streaky patterns as seen in Fig. 13(c), although their scales are considerably larger than those for the forced convection. These patterns are similar to those found by the authors [6] in the turbulent boundary layer of pure natural convection. Their normalized streak spacing $\hat{\lambda}$ $[= (g\beta q\lambda^4/\kappa\nu^2)_w^{1/4}]$ becomes 55, and this value coincides fairly well with that described in the above work. On the other hand, in the combined convection region shown in Fig. 13(b), a reduced number of streaks and much larger spacing between them is observed.

In order to obtain the quantitative information on these streaks, the averaged spanwise spacing λ between the adjacent pairs of streaks, and the frequencies of streaks f which pass a fixed point of the surface, were measured from a number of these photos. The liquid crystal sheet utilized here changes

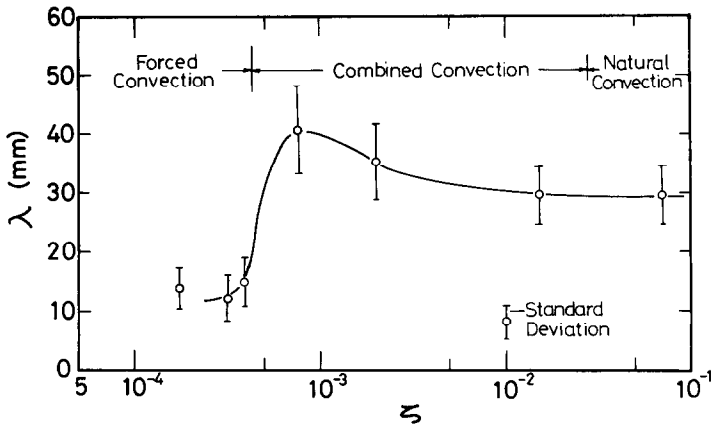

FIG. 14. Streamwise spacing between the streaks measured from the visual data.

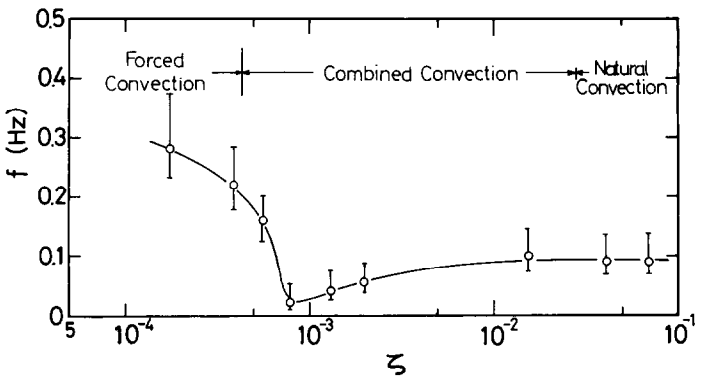

FIG. 15. Frequencies of streaks measured from the visual data.

the color in the temperature range 35–40°C. The typical examples of the spacing λ and frequencies f are illustrated in Figs. 14 and 15, respectively, where the parameter ζ $(= Grx^*/NuxRex^{2.7})$ is adopted as an abscissa. Figure 14 indicates that λ, which is the smallest in the forced convection region, increases rapidly with a slight increase in ζ and reaches the maximum in the combined convection region, and then gradually decreases with further increase in ζ. The minimum value of the frequency f appears also in the combined convection region as is shown in Fig. 15.

These data reveal that the generation and the passage of the low temperature streaks are retarded significantly in the combined convection region. Considering the fact that the visualized patterns represent the instantaneous distributions of the local heat transfer rates, the above result qualitatively well explains the reduced heat transfer mentioned in Section 3.1. However, the Nusselt numbers in the combined convection region become smaller by only 25% than those for the pure forced convection, despite such marked reductions in the streaky patterns. This may be due, in part, to the acceleration of the flow near the wall. Further studies are needed to investigate the quantitative correlations between these streaky patterns and the heat transfer.

The above streaky patterns are considered to reflect the successive motion of the fluid lumps which exist in the near-wall region of the boundary layer. Therefore, the visualization of the flow field near the wall was performed to investigate the relations between the fluid motion and the streaky patterns. Figures 16(a)–(c) show a representative set of visualized data in each region of forced, combined and natural convection, respectively. The hydrogen-bubble method was employed here, and the cathode wire was stretched horizontally at $Y = 2.1$ mm from the wall and at a height $X = 2.6$ m. These photos were taken from the locations where the flow field could be observed stereoscopically.

As is apparent from the result with the forced convection presented in Fig. 16(a), the time-lines of bubbles show the non-uniform velocity distribution in the spanwise direction. Here, f_1 the portions of high streamwise velocity $(u' > 0)$ are recessed to the wall $(v' < 0)$, and f_2 the portions of low velocity $(u' < 0)$ are ejected from the wall $(v' > 0)$. The above fluid motion of f_1 and f_2 can be referred as the sweep and ejection stages of the bursting phenomena, respectively, and have been revealed by Kline *et al.* [7] in the turbulent boundary layer of pure forced convection. In the natural convection region, the fluid motion which consists of n_1 the low velocity $(u' < 0)$ inflow toward the wall $(v' < 0)$, and of n_2 the high velocity $(u' > 0)$ outward flow from the wall $(v' > 0)$, is observed in Fig. 16(c). The fluid motion of n_1 and n_2 has also been found in the turbulent boundary layer of pure natural convection by the previous work of the authors [6]. It should be considered from these photos that the low temperature streaks in the forced and natural convection, which were shown in Figs. 13(a) and (c), are generated by the fluid motions of f_1 and n_1, respectively. They convey the low temperature fluid lumps to the wall, while the high surface temperature appears in the regions where the fluid motions of f_2 and n_2 take place. Thus, the streaky patterns in the surface temperatures are correlated with the fluid motion.

Meanwhile, in the combined convection region shown in Fig. 16(b), the time-lines of the bubbles become flat, and the intervals between the time-lines are fairly uniform in the spanwise direction. This result confirms that the velocity fluctuations u' and v' are most suppressed in the combined convection region. Furthermore, the distinguished fluid motion, such as the bursting phenomena as in a forced convection, can scarcely be observed. This result also well accounts for the reduced numbers of the low temperature streaks.

It should be noted from these visual data that the fluid motions of f_1 and f_2 in the forced convection region and of n_1 and n_2 in the natural convection region make an opposite contribution to the turbulent transport. Although it is rather qualitative to deduce the following results, the former fluid motion of f_1 and f_2 will provide the positive values of Reynolds shear stress $-\rho u'v'$, while the negative values of $-\rho u'v'$ will be yielded by the latter fluid motion, n_1 and n_2. Therefore, their interaction may result in the minimum absolute values of the Reynolds shear stress and, thus, the turbulent production will be seriously

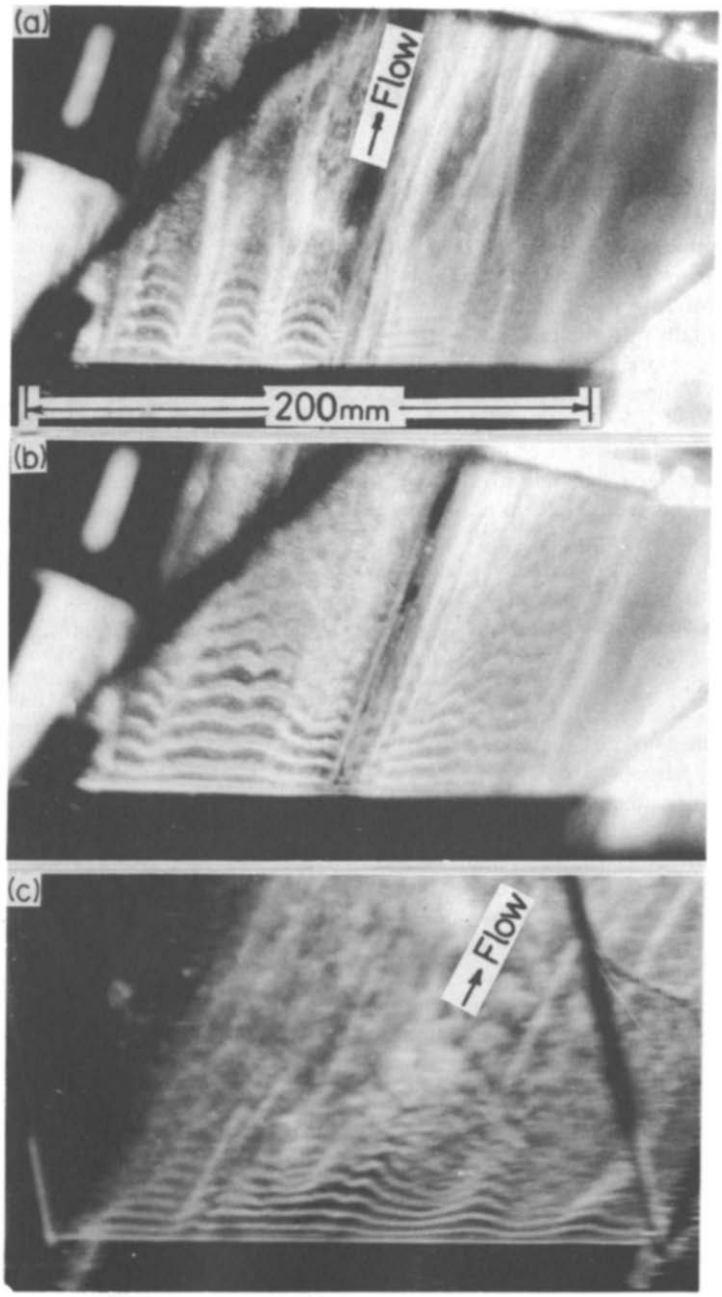

FIG. 16. Visualization of the flow field in the near wall region by the hydrogen-bubble method. (a) Forced convection: $U_\infty = 9.6\,\mathrm{cm\,s^{-1}}$, $q_w = 650\,\mathrm{W\,m^{-2}}$, $Rex = 2.50 \times 10^5$, $Grx^* = 0.82 \times 10^{14}$, $\zeta = 1.48 \times 10^{-4}$. (b) Combined convection: $U_\infty = 9.6\,\mathrm{cm\,s^{-1}}$, $q_w = 4000\,\mathrm{W\,m^{-2}}$, $Rex = 2.48 \times 10^5$, $Grx^* = 9.75 \times 10^{14}$, $\zeta = 2.12 \times 10^{-3}$. (c) Natural convection: $U_\infty = 2.6\,\mathrm{cm\,s^{-1}}$, $q_w = 4000\,\mathrm{W\,m^{-2}}$, $Rex = 7.30 \times 10^4$, $Grx^* = 9.98 \times 10^{14}$, $\zeta = 4.70 \times 10^{-2}$.

inhibited in the combined convection region. The nonviolent fluid motion shown in Fig. 16(b) may suggest the occurrence of the above interaction. Quantitative measurements are needed to confirm the above, however, the present visual data can afford definite pictures of the turbulent transport within the combined convective boundary layers.

4. CONCLUDING REMARKS

The present study has been conducted to investigate experimentally the transport mechanisms of heat and momentum within a turbulent boundary layer of combined convection. The experiments were performed on an aiding flow of water induced by both

forced convection and natural convection along a vertical flat plate, heated with a uniform heat flux.

The local heat transfer coefficients in the vertical direction were measured in the range of high Rayleigh and Reynolds numbers up to the maximum $Rax^* \simeq 6 \times 10^{16}$ and $Rex \simeq 10^6$. It was revealed that the local Nusselt numbers decrease as much as 25% than those for the pure natural convection as well as for the pure forced convection, in a certain range of Rax^* and Rex numbers. This reduction in heat transfer was found to occur when the parameter ζ $[= Grx^*/NuxRex^{2.7}]$ falls into the region, $4 \times 10^{-4} < \zeta < 3 \times 10^{-2}$. Furthermore, the forced, the natural and the combined convection regions are classified in terms of the value ζ.

The quantitative data of time-averaged velocity and temperature and also of their fluctuation intensities were measured in each flow regime. It was found that the turbulent fluctuations are suppressed markedly in the combined convection region. This result indicates that the reductions in heat transfer are attributable to the turbulence suppression.

The temperature and flow fields over the test plate were visualized to investigate the turbulent transport mechanisms within the combined convective boundary layers. The surface temperature distributions, which were visualized by using a liquid crystal sheet, reveal that the generation and the passage of the low temperature streaks are most reduced in the combined convection region. These results with the streaky patterns are correlated well with the heat transfer behavior. The hydrogen-bubble method was also adopted to visualize the fluid motion in the near-wall region of the boundary layer. It was revealed that the distinguished fluid motion, which appears in both boundary layers of the forced and natural convection, can scarcely be observed in the combined convection region. The visualized results also confirm that the velocity fluctuations u' and v' are most suppressed in the combined convection region. Furthermore, the turbulent transport within the boundary layers was discussed from these visual data.

Acknowledgement—The authors wish to acknowledge the financial support from the Ministry of Education, Science, and Culture of Japan through a research grant (No. 59750151).

REFERENCES

1. W. B. Hall and P. H. Price, Mixed forced and free convection from a vertical heated plate to air, *Proc. 4th Int. Heat Transfer Conference*, Vol. 3, NC.3.3 (1970).
2. P. H. Oosthuizen, Turbulent combined convective flow over a vertical plane surface, *Proc. 5th Int. Heat Transfer Conference*, Vol. 3, NC.4.1, pp. 129–133 (1974).
3. B. S. Petukhov and B. K. Sporygin, Experimental study of heat transfer in a viscous inertial gravitational liquid flow in vertical tubes, *Teplofiz. Vysok. Temp.* **6**, 933–937 (1968).
4. M. J. Watts and C. T. Chou, Mixed convection heat transfer to supercritical pressure water, *Proc. 7th Int. Heat Transfer Conference*, Vol. 3, MC16, pp. 495–500 (1982).
5. B. S. Petukhov, A. F. Polyakov and O. G. Martynenko, Buoyancy effect on heat transfer in forced channel flows, *Proc. 7th Int. Heat Transfer Conference*, Vol. 1, RK5, pp. 343–362 (1982).
6. K. Kitamura, M. Koike, I. Fukuoka and T. Saito, Large eddy structure and heat transfer of turbulent natural convection along a vertical flat plate, *Int. J. Heat Mass Transfer* **28**, 837–850 (1985).
7. S. J. Kline, W. C. Reynolds, F. A. Schraub and P. W. Rundstadler, The structure of turbulent boundary layer, *J. Fluid Mech.* **30**, 741–773 (1967).
8. T. Fujii, M. Takeuchi, M. Fujii, K. Suzaki and H. Uehara, Experiments on natural-convection heat transfer from the outer surface of a vertical cylinder to liquid, *Int. J. Heat Mass Transfer* **13**, 753–783 (1970).
9. G. C. Vliet and C. K. Liu, An experimental study of turbulent natural convection boundary layer, *Trans. Am. Soc. mech. Engrs*, Series C, *J. Heat Transfer* **91**, 517–531 (1969).
10. D. R. Chapman and M. W. Rubesin, Temperature and velocity profiles in the compressible laminar boundary layer with arbitrary distribution of surface temperature, *J. aeronaut. Sci.* **16**, 547–565 (1949).
11. R. G. Deissler, Analysis of turbulent heat transfer, mass transfer, and friction in smooth tubes at high Prandtl and Schmidt numbers, NACA Rep. 1210 (1954).
12. Y. Katto, *Dennetsu Gairon* (*Outline of Heat Transfer*). Yokendo, Tokyo (1964), in Japanese.
13. W. C. Reynolds, W. M. Kays and S. J. Kline, A summary of experiments on turbulent heat transfer from a non-isothermal flat plate, *Trans. Am. Soc. mech. Engrs*, Series C, *J. Heat Transfer* **82**, 341–348 (1960).
14. B. A. Kader and A. M. Yaglom, Heat and mass transfer laws for fully turbulent wall flows, *Int. J. Heat Mass Transfer* **15**, 2329–2351 (1972).
15. P. H. Oosthuizen and R. Hart, A numerical study of laminar combined convective flow over flat plates, *Trans. Am. Soc. mech. Engrs*, Series C, *J. Heat Transfer* **95**, 60–63 (1973).
16. N. Kasagi, Liquid crystal application in heat transfer experiments, IL-27, Thermoscience Division, Mechanical Engineering Department, Stanford University, Stanford, CA (1980).
17. Y. Iritani, N. Kasagi and M. Hirata, Transport mechanisms within turbulent boundary layer over a flat plate (first report), *Trans. Japan Soc. mech. Engrs* **38**, 2284–2294 (1982), in Japanese.

TRANSFERT TURBULENT DE CHALEUR ET DE QUANTITE DE MOUVEMENT POUR UNE CONVECTION MIXTE LE LONG D'UNE PLAQUE PLANE VERTICALE—ECOULEMENT AIDE

Résumé—On étudie expérimentalement un écoulement turbulent mixte aidé le long d'une plaque plane verticale dans le domaine des grands nombres Ra_x^* et Re_x. Des nombres de Nusselt locaux dans la région de convection mixte sont trouvés inférieurs, jusqu'à 25%, que ceux de la convection pure forcée et naturelle. On trouve à partir des mesures de vitesse et de température que les réductions de transfert de chaleur sont principalement causées par une suppression de turbulence. Les mécanismes de transport dans les couches limites de convection mixte sont discutés à partir des visualisations des champs de vitesse et de température sur la plaque.

TURBULENTER WÄRME- UND IMPULSTRANSPORT BEI KOMBINIERTER NATÜRLICHER UND DAZU GLEICHGERICHTETER ERZWUNGENER KONVEKTION ENTLANG EINER SENKRECHTEN PLATTE

Zusammenfassung—Die turbulente natürliche und dazu gleichgerichtete erzwungene Konvektion entlang einer senkrechten ebenen Platte wird experimentell im Bereich hoher Rayleigh- und Reynolds-Zahlen (beide bezogen auf die Lauflänge) untersucht. Es zeigt sich, daß die örtliche Nusselt-Zahl bis zu 25% geringer ist als bei reiner natürlicher und reiner erzwungener Konvektion. Die Messungen von Geschwindigkeit und Temperatur zeigen, daß diese Verringerung beim Wärmeübergang vor allem durch die Unterdrückung der Turbulenz hervorgerufen wird. Turbulente Transportmechanismen innerhalb der kombinierten konvektiven Grenzschichten werden auch auf der Basis der Strömungs- und Temperaturfelder diskutiert.

ТУРБУЛЕНТНЫЙ ПЕРЕНОС ТЕПЛА И КОЛИЧЕСТВА ДВИЖЕНИЯ СОВМЕСТНОЙ ВЫНУЖДЕННОЙ И ЕСТЕСТВЕННОЙ КОНВЕКЦИЕЙ ПРИ ОБТЕКАНИИ ПЛОСКОЙ ПЛАСТИНЫ СПУТНЫМ ПОТОКОМ

Аннотация—Проведено экспериментальное исследование спутного потока при турбулентной смешанной конвекции у вертикальной плоской пластины в диапазоне больших чисел Рэлея и Рейнольдса. Найдено, что локальные значения числа Нуссельта в области смешанной конвекции снижаются на 25% по сравнению с числами Нуссельта для чисто вынужденной и чисто естественной конвекции. Результаты измерений скорости и температуры показывают, что снижение интенсивности переноса тепла происходит в основном из-за подавления турбулентности. Используя данные, полученные при визуализации полей течения и температуры для исследуемой пластины, рассмотрены также механизмы турбулентного переноса в пограничных слоях при смешанной конвекции.